ELSEVIER

Inorganica Chimica Acta 226 (1994) 1–8

Inorganica Chimica Acta

The redox behaviour of the cluster anion $[Fe_4N(CO)_{12}]^-$. Electron transfer chain catalytic substitution reactions. Crystal structure of $[Fe_4N(CO)_{11}PPh_3)]^-$

Piero Zanello [a,*], Franco Laschi [a], Arnaldo Cinquantini [a], Roberto Della Pergola [b], Luigi Garlaschelli [b], Mario Cucco [b], Francesco Demartin [c,*], Trevor R. Spalding [d]

[a] *Dipartimento di Chimica dell'Università di Siena, Piano dei Mantellini 44, I-53100 Siena, Italy*

[b] *Dipartimento di Chimica Inorganica e Metallorganica dell'Università di Milano, Via G. Venezian 21, I-20133 Milan, Italy*

[c] *Istituto di Chimica Strutturistica Inorganica dell'Università di Milano, Via G. Venezian 21, I-20133 Milan, Italy*

[d] *Department of Chemistry, University College, Cork, Ireland*

Received 31 March 1994

Abstract

The electrochemical investigation of the redox properties of the monoanion $[Fe_4N(CO)_{12}]^-$ points out its ability to undergo sequentially two one-electron reductions. The first step leads to the quite stable dianion $[Fe_4N(CO)_{12}]^{2-}$; the EPR results indicate that in frozen solution an equilibrium exists between two different molecular geometries of such a dianion. The second electron addition produces the relatively short-lived trianion $[Fe_4N(CO)_{12}]^{3-}$. In the presence of monodentate phosphines, the redox change $[Fe_4N(CO)_{12}]^{-/2-}$ triggers the electrocatalytic substitution of one CO group to afford the substituted monoanions $[Fe_4N(CO)_{11}(PR_3)]^-$. As a matter of fact, sub-stoichiometric amounts of $Ph_2CO^{\bullet-}$ produce $[Fe_4N(CO)_{11}(PPh_3)]^-$, the crystal structure of which has been solved. Crystal data for $[N(PPh_3)_2][Fe_4N(CO)_{11}(PPh_3)]$: triclinic, space group $P\bar{1}$ (No. 2), $a = 11.009(6)$, $b = 17.285(4)$, $c = 17.380(2)$ Å, $\alpha = 103.11(3)$, $\beta = 91.18(2)$, $\gamma = 105.26(3)°$, $Z = 2$, $D_c = 1.444$ g cm^{-3}, Mo Kα radiation ($\lambda = 0.71073$ Å), μ(Mo Kα) = 10.5 cm^{-1}, $R = 0.048$ ($R_w = 0.054$) for 5010 independent reflections having $I > 3\sigma(I)$. Preliminary evidence is given that in the presence of bidentate phosphines one CO ligand substitution occurs at room temperature, whereas two CO groups are replaced at higher temperatures.

Keywords: Crystal structures; Electrochemistry; Iron complexes; Carbonyl complexes; Nitrido complexes; Cluster complexes

1. Introduction

The ability of metal–sulfur [1,2] and metal–carbonyl [3,4] cluster assemblies to undergo reversibly multiple electron transfers is well documented.

With reference to the special class of carbonyl cluster compounds containing interstitial or exposed heteroatoms, after having reported on the electron-transfer ability of the pentairon-nitrido anion $[Fe_5N(CO)_{14}]^-$ [5], we thought to study the electrochemical behaviour of the tetrairon-nitrido anion $[Fe_4N(CO)_{12}]^-$ [6,7]. In addition, the recent preparation of the monosubstituted complex $[Fe_4N(CO)_{11}(PMe_2Ph)]^-$ by thermal activation [8], induced us to examine the possibility of obtaining such phosphino-substituted complexes by electrochemically induced electron transfer chain (ETC) catalysis (electrocatalysis) [9], which has well grounded precedents in tri-iron [10–12], as well as in tricobalt [13,14] and tetra-cobalt [15] carbonyl species.

2. Results and discussion

2.1. Electrochemistry

Fig. 1 shows the cyclic voltammetric response exhibited by $[Fe_4N(CO)_{12}]^-$ in acetonitrile solution. Two consecutive reduction processes are shown, each of which displays a directly associated response in the reverse scan. Controlled potential coulometry proved they involve one-electron/molecule. Cyclic voltammetric tests run after exhaustive electrolyses showed that the first $-/2-$ cathodic step is chemically reversible, whereas the second $2-/3-$ step leads to slow irre-

* Corresponding authors.

SSDI 0020-1693(94)04061-Y

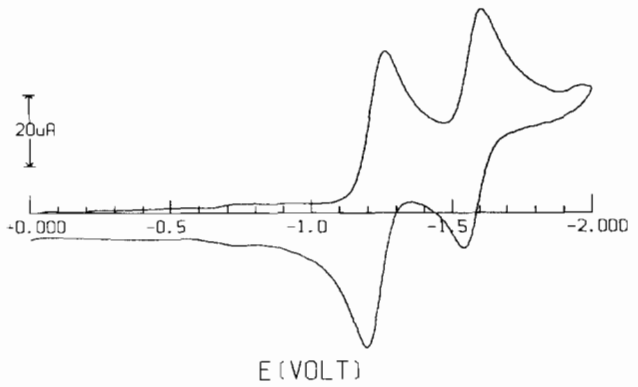

Fig. 1. Cyclic voltammogram recorded at a mercury electrode on a MeCN solution containing $[NEt_4][Fe_4N(CO)_{12}]$ (1.6×10^{-3} mol dm^{-3}) and $[NEt_4][ClO_4]$ (0.2 mol dm^{-3}). Scan rate 0.2 V s^{-1}.

Table 1
Formal electrode potentials (V vs. SCE) for the two sequential one-electron additions exhibited by $[Fe_4N(CO)_{12}]^-$ and $[Fe_5N(CO)_{14}]^-$, at a mercury electrode, in different non-aqueous solutions

Complex	Reduction		Oxidation	Solvent
	$E^{\circ\prime}$ −/2−	$E^{\circ\prime}$ 2−/3−	E_p	
$[Fe_4N(CO)_{12}]^-$	−1.23	−1.58[b]	+0.65	MeCN
	−1.33	−1.74[b]	+0.78	THF
	−1.37[b]	−1.71[b]	+0.44[b,c]	CH_2Cl_2
$[Fe_5N(CO)_{14}]^-$	−0.90	−1.40[a]	+0.70	MeCN
	−0.97	−1.55[a]	+0.60	THF
	−1.04[b]	−1.50[a]	+0.64	CH_2Cl_2

[a]Complicated by fast chemical reactions.
[b]Complicated by slow chemical reactions.
[c]Displaying some features of chemical reversibility.

versible cluster degradation.

A multielectron irreversible oxidation process can be put in evidence at a platinum electrode.

It must be taken into account that some slight poisoning effects take place either at mercury or platinum electrodes, thus making necessary surface cleanings from time to time.

The change of solvent from acetonitrile to tetrahydrofuran does not change the redox profile, but, as it happens for $[Fe_5N(CO)_{14}]^-$ [5], in dichloromethane solution the electrogenerated dianion $[Fe_4N(CO)_{12}]^{2-}$ undergoes slow degradation.

Table 1 summarizes the electrode potentials of the redox changes displayed by $[Fe_4N(CO)_{12}]^-$, also in comparison with those exhibited by the related $[Fe_5N(CO)_{14}]^-$. It is evident that the addition of electrons to $[Fe_4N(CO)_{12}]^-$ is significantly more difficult than that to $[Fe_5N(CO)_{14}]^-$, thus indicating that the LUMO level of the former is significantly higher in energy than that of the latter.

2.2. EPR analysis

Even if the paramagnetic species $[Fe_4N(CO)_{12}]^{2-}$ proved to be quite stable, we electrogenerated it at low temperature (−15 °C) for EPR analysis in order to prevent eventual minor decomposition reactions.

Fig. 2 shows the X-band EPR spectra of $[Fe_4N(CO)_{12}]^{2-}$ in acetonitrile solution both at liquid nitrogen (a) and room (b) temperature, respectively. Three well separated signals exhibiting different g values, linewidths and spectral intensities are present under glassy solution conditions ($T=100$ K), whereas at room temperature ($T=300$ K) the anisotropic features quickly collapse to a single, relatively narrow, unresolved signal ($g_{iso}=2.015\pm0.005$; $\Delta H_{iso}=6\pm0.3$ G). This behaviour is reversible with temperature. These data can be suitably interpreted assuming that at low temperature the $S=1/2$ paramagnetic metal dianion assumes two different geometries, hereafter indicated as A and B, respectively. Based on the relevant spectral intensities, the A/B system appears in a 1:4 ratio. Second derivative analysis and a computer simulation (SIM14a program) [16] allow attribution of the low-field and high-field liquid nitrogen signals to the parallel and perpendicular absorption of the most abundant paramagnetic species A ($g_{\parallel}=2.060\pm0.005$; $g_{\perp}=1.998\pm0.005$; $\langle g\rangle=1/3(g_{\parallel}+2g_{\perp})=2.019\pm0.005$), whereas the intermediate signal is assigned to the poorly resolved axial structure of B ($g_{\parallel}=2.033\pm0.005$; $g_{\perp}=2.020\pm0.005$; $\langle g\rangle=$

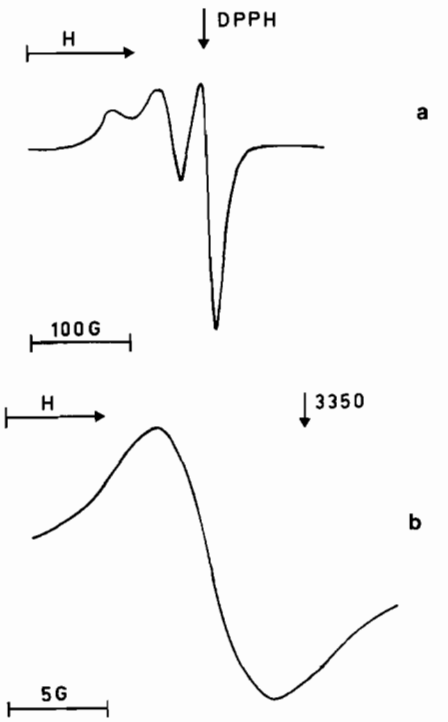

Fig. 2. X-band EPR spectra of the MeCN solution of $[Fe_4N(CO)_{12}]^{2-}$ recorded at 100 K (a) and room temperature (b).

2.025 ± 0.005). The present EPR spectra did not reveal any hyperfine coupling of the $S = 1/2$ electron with the nitrogen atom of the cluster framework; this is not surprising in view of the noticeable metal character of the A/B systems, as pointed out by their lineshapes either at liquid nitrogen or room temperature. In particular, the ΔH_{iso} (300 K) (Fig. 2(a)) can be assumed as the upper value for the hyperfine coupling (if any) of the unpaired electron with the N nucleus:

$$\Delta H_{iso}(300\ K) = 6 \pm 0.3\ G > a_{iso}(N)$$

2.3. Electrochemically induced electrocatalytic ligand substitution in $[Fe_4N(CO)_{12}]^-$

Fig. 3 shows the cyclic voltammogram exhibited by $[Fe_4N(CO)_{12}]^-$ under the experimental conditions of Fig. 1, but in the presence of an excess of PPh_3 (at potentials higher than -0.5 V ($E_p = -0.22$ V) an oxidation process attributable to the formation of mercury–phosphino complexes takes place).

The presence of the phosphine causes the appearance of a new irreversible cathodic process ($E_p = -1.45$ V) in between the two sequential $-/2-/3-$ reductions. Controlled potential coulometry at the first cathodic step ($E_w = -1.25$ V) is now completed in a few minutes and 0.05 clcctrons/molecule are spent. Cyclic voltammetric tests after exhaustive electrolysis only reveal the presence of the irreversible peak at $E_p = -1.45$ V, which is hence attributable to the reduction of the electrogenerated anion $[Fe_4N(CO)_{11}(PPh_3)]^-$. These data are clearly indicative of the occurrence of the following electrocatalytic cycle [9].

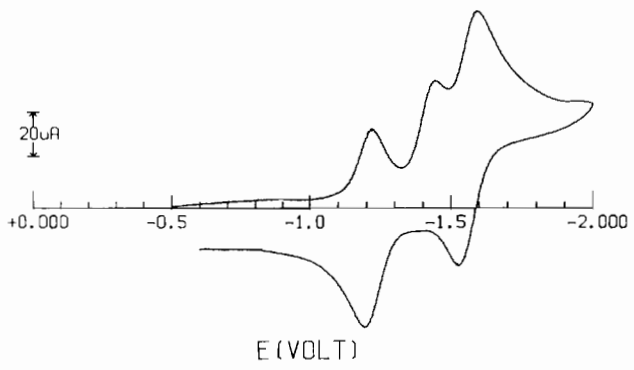

Fig. 3. Cyclic voltammogram recorded at a mercury electrode on a MeCN solution containing $[Fe_4N(CO)_{12}]^-$ (1.6×10^{-3} mol dm^{-3}) and PPh_3 (9.5×10^{-3} mol dm^{-3}). $[NEt_4][ClO_4]$ supporting electrolyte (0.2 mol dm^{-3}). Scan rate 0.2 V s^{-1}.

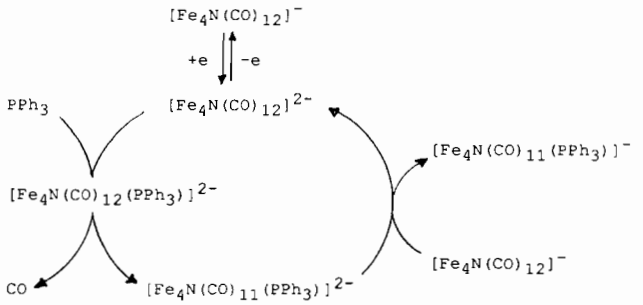

The driving force of the electrocatalytic process, as measured by the separation between the redox potentials of the steps $[Fe_4N(CO)_{12}]^-/[Fe_4N(CO)_{12}]^{2-}$ and $[Fe_4N(CO)_{11}(PPh_3)]^-/[Fe_4N(CO)_{11}(PPh_3)]^{2-}$ [9] is of about 5 kcal mol^{-1}.

A preliminary monitoring of the IR spectrum of the exhaustively electrolyzed solution showed that the major ν(CO) bands of the original monoanion (in MeCN, 2010s, 1993vs cm^{-1}) were significantly affected by phosphine substitution (2030s, 1990w, 1975vs cm^{-1}).

Only recently, the electrocatalytic CO substitution by P-donors in $[(C_5H_4Me)Mn(CO)_2(NO)]^+$ has been shown to depend significantly on the temperature [17]. In this connection, Fig. 4 shows the cyclic voltammograms recorded at different temperatures on a 1:3 mixture of $[Fe_4N(CO)_{12}]^-$ and PPh_3. These data can be interpreted by considering that the rate of CO release, in the activated complex, increases with temperature [17].

A further interesting aspect of such temperature-induced CO activation is shown in Fig. 5, which shows the cyclic voltammetric responses exhibited by $[Fe_4N(CO)_{12}]^-$ in the presence of the bidentate 1,2-bis(diphenylphosphino)ethane (dppe) at diffcrcnt temperatures.

As can be seen, up to +20 °C the voltammetric behaviour quite parallels that of the monodentate phosphine PPh_3 (with the appearance of a new peak at $E_p = -1.45$ V), but at +30 °C a further cathodic peak appears at more negative potentials ($E_p = -1.75$ V). This is likely associated with the fact that at low temperatures, the diphosphine, acting as a monodentate ligand, substitutes only one CO group affording $[Fe_4N(CO)_{11}(dppe)]^-$, whereas at higher temperatures two carbonyls are replaced to afford $[Fe_4N(CO)_{10}(dppe)]^-$.

Such a behaviour was also displayed by bis(diphenylphosphino)methane as well as 1,3-bis(diphenylphosphino)propane. In contrast, both 1,2-bis(dimethylphosphino)ethane and the tripodal triphosphine $MeC(CH_2PPh_2)_3$ do not induce CO substitution. More extensive investigations will be reported in the future.

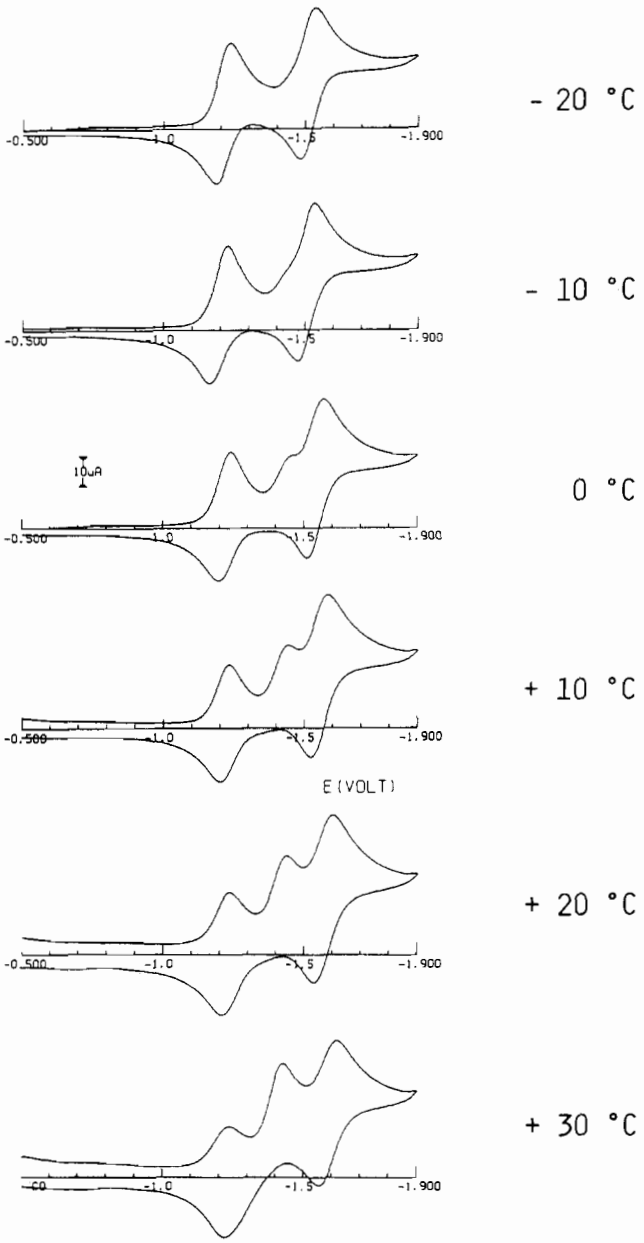

Fig. 4. Cyclic voltammetric responses recorded at different temperatures on a MeCN solution containing $[Fe_4N(CO)_{12}]^-$ (1.1×10^{-3} mol dm^{-3}) and PPh_3 (3.4×10^{-3} mol dm^{-3}). $[NEt_4][ClO_4]$ supporting electrolyte (0.2 mol dm^{-3}). Mercury working electrode. Scan rate 0.2 V s^{-1}.

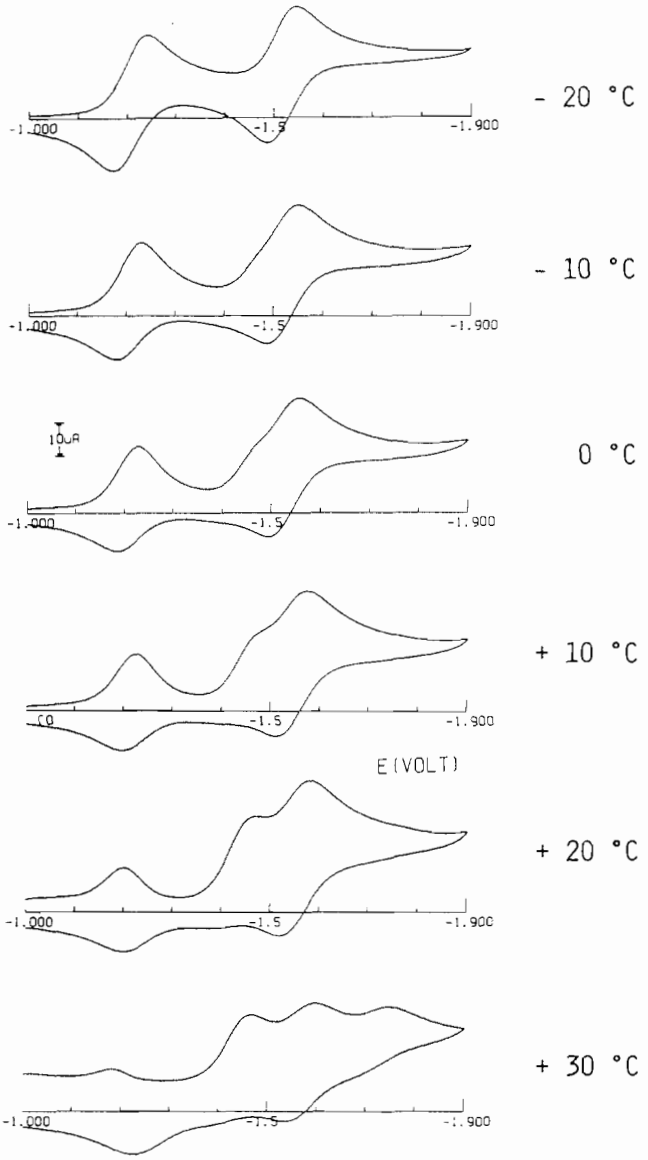

Fig. 5. Cyclic voltammetric responses recorded at different temperatures on a MeCN solution containing $[Fe_4N(CO)_{12}]^-$ (1.1×10^{-3} mol dm^{-3}) and dppe (1.0×10^{-2} mol dm^{-3}). $[NEt_4][ClO_4]$ supporting electrolyte (0.2 mol dm^{-3}). Mercury working electrode. Scan rate 0.2 V s^{-1}.

2.4. Chemical preparation of $[Fe_4N(CO)_{11}(PPh_3)]^-$

In order to test the electrochemical evidence, we prepared the monosubstituted species $[Fe_4N(CO)_{11}(PPh_3)]^-$ by simply adding a THF solution of sodium diphenylketyl to a THF solution of $[N(PPh_3)_2][Fe_4N(CO)_{12}]$ containing PPh_3 in about 1:1 ratio. In order to drive the reaction to completeness it was necessary to add gradually almost a half mole of reductant per mole of cluster. Selected crystals of $[N(PPh_3)_2][Fe_4N(CO)_{11}(PPh_3)]$ show bands in the CO stretching region at 2036w, 1984s, 1970s and 1931w (cm^{-1}, THF solution). This spectrum, compared with that of the parent carbonyl compound, suggests a reduced molecular symmetry of the product, in agreement with the substitution of one carbonyl ligand with PPh_3. Further confirmation of the formation of $[Fe_4N(CO)_{11}(PPh_3)]^-$ comes from the ^{31}P NMR spectrum which shows a resonance at 67.53 ppm (THF-d_8 solution).

A preliminary examination of the reaction in the presence of dppe afforded a product showing IR bands (in THF) at 2036w, 1985s, 1969vs and 1941m (cm^{-1}, THF solution). The remarkable similarity with the

spectrum of $[Fe_4N(CO)_{11}(PPh_3)]^-$ suggests the formation of $[Fe_4N(CO)_{11}(dppe)]^-$, where the diphosphine acts as a monodentate ligand. Any attempt to grow crystals was unsuccessful.

2.5. X-ray characterization of $[Fe_4N(CO)_{11}(PPh_3)]^-$

The molecular structure of the $[Fe_4N(CO)_{11}(PPh_3)]^-$ anion is shown in Fig. 6, together with the atom-numbering scheme adopted; selected interatomic distances and angles are reported in Table 2.

With respect to the original monoanion $[Fe_4N(CO)_{12}]^-$, the phosphine ligand replaces one carbonyl on the wingtip, less coordinated iron vertex. Among the three carbonyls which may undergo substitution, one is unique (there is no Fe–Fe interaction almost *trans* to it) and shows the longest Fe–C bond (here Fe(2)–C(21), 1.805(9) Å or Fe(4)–C(41), 1.806(5) Å). Nevertheless, the replacement occurs at one of the remaining two equivalent carbonyls which lie approximately in the plane of an iron triangle. This behaviour is strongly reminiscent of what happens in the $M_2(CO)_{10}$ complexes (M = Mn, Re), where the axial CO, with shorter $M–CO_{axial}$ distances, are preferentially substituted [18], although it is believed that CO dissociates from the equatorial sites, in agreement with longer $M–CO_{equatorial}$ bonding distances [19]. Probably, steric hindrance of the substituting ligand is the driving force for the actual situation. Certainly, in $[Fe_4N(CO)_{11}(PPh_3)]^-$ a degree of steric overcrowding is still present: the shortest intramolecular contact refers to the phenyl rings C(111)–C(116) with CO(41) and CO(42), and C(131)–C(136) with CO(32) and CO(33). Even the C–Fe–P angles seem to be affected by these

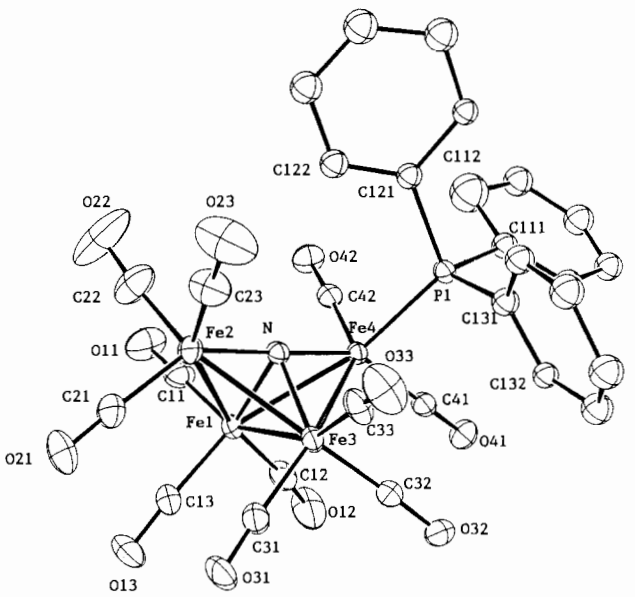

Fig. 6. Perspective view of the monoanion $[Fe_4N(CO)_{11}(PPh_3)]^-$.

Table 2
Selected interatomic distances (Å) and angles (°)

Fe1–Fe2	2.594(1)	Fe2–Fe3	2.589(1)
Fe1–Fe3	2.507(1)	Fe3–Fe4	2.651(1)
Fe1–Fe4	2.593(1)		
Fe1–N	1.922(5)	Fe2–N	1.778(5)
Fe3–N	1.879(5)	Fe4–N	1.771(5)
Fe1–C11	1.773(7)	C11–O11	1.158(9)
Fe1–C12	1.777(6)	C12–O12	1.147(8)
Fe1–C13	1.771(8)	C13–O13	1.15(1)
Fe2–C21	1.805(9)	C21–O21	1.14(1)
Fe2–C22	1.745(8)	C22–O22	1.13(1)
Fe2–C23	1.747(8)	C23–O23	1.16(1)
Fe3–C31	1.781(8)	C31–O31	1.15(1)
Fe3–C32	1.759(6)	C32–O32	1.156(7)
Fe3–C33	1.793(7)	C33–O33	1.154(9)
Fe4–C41	1.806(5)	C41–O41	1.140(6)
Fe4–C42	1.736(6)	C42–O42	1.169(8)
Fe4–P1	2.217(2)		
P1–C111	1.838(7)		
P1–C121	1.820(5)		
P1–C131	1.825(6)		
Fe2–Fe1–Fe3	60.99(3)	Fe1–Fe2–C23	152.3(3)
Fe2–Fe1–Fe4	86.30(4)	Fe3–Fe2–N	46.5(2)
Fe2–Fe1–N	43.3(1)	Fe3–Fe2–C21	103.1(2)
Fe2–Fe1–C11	94.8(2)	Fe3–Fe2–C22	150.4(3)
Fe2–Fe1–C12	163.1(3)	Fe3–Fe2–C23	100.5(2)
Fe2–Fe1–C13	93.1(2)	N–Fe2–C21	143.8(3)
Fe3–Fe1–Fe4	62.63(4)	N–Fe2–C22	105.2(3)
Fe3–Fe1–N	48.0(1)	N–Fe2–C23	105.3(3)
Fe3–Fe1–C11	151.3(2)	C21–Fe2–C22	98.8(4)
Fe3–Fe1–C12	102.9(3)	C21–Fe2–C23	98.9(4)
Fe3–Fe1–C13	97.3(2)	C22–Fe2–C23	95.5(4)
Fe4–Fe1–N	43.1(1)	Fe1–Fe3–Fe2	61.18(3)
Fe4–Fe1–C11	103.4(3)	Fe1–Fe3–Fe4	60.27(4)
Fe4–Fe1–C12	80.9(3)	Fe1–Fe3–N	49.5(2)
Fe4–Fe1–C13	157.2(2)	Fe1–Fe3–C31	95.6(2)
N–Fe1–C11	104.2(3)	Fe1–Fe3–C32	101.7(2)
N–Fe1–C12	122.7(3)	Fe1–Fe3–C33	155.3(2)
N–Fe1–C13	131.2(3)	Fe2–Fe3–Fe4	85.19(4)
C11–Fe1–C12	98.9(3)	Fe2–Fe3–N	43.4(1)
C11–Fe1–C13	99.3(4)	Fe2–Fe3–C31	90.2(2)
C12–Fe1–C13	94.4(3)	Fe2–Fe3–C32	161.7(2)
Fe1–Fe2–Fe3	57.84(3)	Fe2–Fe3–C33	96.5(2)
Fe1–Fe2–N	47.8(2)	Fe4–Fe3–N	41.8(1)
Fe1–Fe2–C21	102.7(2)	Fe4–Fe3–C31	154.4(2)
Fe1–Fe2–C22	98.2(3)	Fe4–Fe3–C32	80.3(2)
Fe4–Fe3–C33	110.5(3)	C111–P1–C121	101.0(3)
N-Fe3–C31	129.2(3)	C111–P1–C131	106.4(3)
N-Fe3–C32	121.5(3)	C121–P1–C131	103.7(3)
N–Fe3–C33	107.4(3)	Fe1–C11–O11	179.7(9)
C31–Fe3–C32	98.2(3)	Fe1–C12–O12	173.7(7)
C31–Fe3–C33	95.0(3)	Fe1–C13–O13	177.0(5)
C32–Fe3–C33	98.9(3)	Fe2–C21–O21	178.3(7)
Fe1–Fe4–Fe3	57.09(4)	Fe2–C22–O22	176(1)
Fe1–Fe4–P1	155.85(6)	Fe2–C23–O23	176.0(8)
Fe1–Fe4–N	47.8(2)	Fe3–C31–O31	176.1(6)
Fe1–Fe4–C41	108.6(2)	Fe3–C32–O32	175.0(6)
Fe1–Fe4–C42	93.9(2)	Fe3–C33–O33	174.6(7)
Fe3–Fe4–P1	106.66(6)	Fe4–C41–O41	179.3(6)
Fe3–Fe4–N	45.0(1)	Fe4–C42–O42	176.5(5)
Fe3–Fe4–C41	107.6(2)	Fe1–N–Fe2	88.9(2)
Fe3–Fe4–C42	146.0(2)	Fe1–N–Fe3	82.5(2)
P1–Fe4–N	108.0(2)	Fe1–N–Fe4	89.1(2)
P1–Fe4–C41	92.9(2)	Fe2–N–Fe3	90.1(2)
P1–Fe4–C42	93.9(2)	Fe2–N–Fe4	176.0(3)
N–Fe4–C41	148.9(3)	Fe3–N–Fe4	93.1(2)
N–Fe4–C42	103.2(2)	Fe4–P1–C121	117.0(2)
C41–Fe4–C42	97.9(3)	Fe4–P1–C131	115.8(2)
Fe4–P1–C111	111.5(2)		

steric effects, and are smaller than the C–Fe–C ones. Steric effects are probably responsible for the elongation of the Fe(3)–Fe(4) distance here and in the other phosphine-substituted analogues, where the longest Fe–Fe distances correspond to a bond with the P-substituted iron atom. The pattern of bond distances and angles within the Fe_4N core is very close to that found for the strictly related monoanion $[Fe_4N(CO)_{11}(PMe_2Ph)]^-$ [8], where the hinge Fe–Fe interaction is 2.504(2) Å (to be compared with the actual value of 2.507(1) Å) and the average Fe–Fe distance in the butterfly wings is 2.603 Å (versus 2.607 Å, here). In the hydride complex $HFe_4N(CO)_{11}(PPh_3)$ the corresponding values are 2.552(1) Å and 2.591 Å, respectively [8]. The former value clearly shows the lengthening effect of the hydride atom bridging the hinge of the butterfly, whereas the latter one is indicative of a slight shortening effect due to the loss of the negative charge upon protonation.

3. Experimental

$[N(PPh_3)_2][Fe_4N(CO)_{12}]$ was prepared according to published procedures [7]. 1,2-Bis(diphenylphosphino)-ethane, bis(diphenylphosphino)methane, 1,3-bis(diphenylphosphino)propane and 1,2-bis(dimethylphosphino) ethane were commercial products (Aldrich).

The materials and apparatus for the electrochemistry and coupled EPR measurements have been described elsewhere [20]. All the potential values are referred to the saturated calomel electrode (SCE). Under the present experimental conditions, the one electron oxidation of ferrocene occurs at +0.38, +0.44 and +0.54 V in acetonitrile, dichloromethane and tetrahydrofuran solution, respectively. The external magnetic field H_0 of the X-band EPR spectrometer was calibrated against a DPPH powder sample ($g_{DPPH} = 2.0036$). IR spectra were recorded on a Perkin-Elmer 16PC Fourier transform spectrophotometer using CaF_2 cells previously purged with dinitrogen. All the solvents were dried and distilled under nitrogen immediately before use. ^{31}P NMR spectra were recorded on a Bruker AC200 spectrometer operating at 200 MHz for hydrogen and are reported downfield from the external standard H_3PO_4 85% in D_2O. All the reactions were conducted under nitrogen atmosphere using the Schlenk tube technique [21].

3.1. Preparation of the sodium diphenylketyl solution

A 0.10 M solution of sodium diphenylketyl was prepared by dissolving 0.091 g (0.5 mmol) of benzophenone in 5 ml of THF, in the presence of a small piece (0.05 g, 2 mmol) of sodium. After a few minutes, under stirring, the solution turned deep blue.

3.2. Preparation of $[N(PPh_3)_2][Fe_4N(CO)_{11}(PPh_3)]$

0.20 g of $[N(PPh_3)_2][Fe_4N(CO)_{12}]$ (0.18 mmol) was dissolved in 20 ml of THF together with 0.048 g of PPh_3 (0.18 mmol) in a ($[N(PPh_3)_2][Fe_4N(CO)_{12}]$:$PPh_3$) 1:1 molar ratio. Five portions of 0.2 ml of sodium diphenylketyl were added, monitoring by IR spectroscopy the solution after each addition. When the molar ratio $[N(PPh_3)_2][Fe_4N(CO)_{12}]$:$Ph_2CO^{\bullet -}$ was about 1:0.5, the reaction was completed. The initial red solution turned brown; the solvent was removed in vacuum and the brown residue was dissolved with 20 ml of MeOH and filtered. The volume of the resulting solution was reduced to one-half and, on standing overnight, well shaped crystals of $[N(PPh_3)_2][Fe_4N(CO)_{11}(PPh_3)]$ were formed. *Anal.* Calc. for $C_{65}H_{45}N_2P_3O_{11}Fe_4$: C, 57.98; H, 3.37; N, 2.08. Found: C, 57.70; H, 3.37; N, 2.23%. The solid compound is fairly air stable; it is soluble in THF, Me_2CO, CH_2Cl_2 and insoluble in aliphatic and aromatic hydrocarbons.

3.3. X-ray data collection and structure determination

Crystal data and other experimental details are summarized in Table 3. A prismatic crystal with approximate dimensions 0.10×0.80×0.20 mm was used. The diffraction measurements were carried out on an Enraf-Nonius CAD4 diffractometer at room temperature, using graphite-monochromatized Mo Kα radiation

Table 3
Crystallographic data

Formula	$C_{65}H_{45}Fe_4N_2O_{11}P_3$
Formula weight	1346.40
Crystal system	triclinic
Space group	$P\bar{1}$
a (Å)	11.009(6)
b (Å)	17.285(4)
c (Å)	17.380(2)
α (°)	103.11(3)
β (°)	91.18(2)
γ (°)	105.26(3)
V (Å^3)	3096(2)
Z	2
D_{calc} (g cm^{-3})	1.444
μ (cm^{-1})	10.5
Min. transmission factor	0.91
Scan mode	ω
ω-Scan width (°)	1.2+0.35 tanθ
θ Range (°)	1–24
Reciprocal space explored	$+h, \pm k, \pm l$
Measured reflections	9810
Unique observed reflections with $I > 3\sigma(I)$	5010
Final R and R_w indices[a]	0.048, 0.054
No. variables	581
GOF[b]	1.76

[a] $R = [\Sigma(F_o - k\|F_c\|)/\Sigma F_o]$; $R_w = [\Sigma w(F_o - k\|F_c\|)^2/\Sigma w F_o^2]^{1/2}$.
[b] $GOF = [\Sigma w(F_o - k\|F_c\|)^2/(N_{obs} - N_{var})]^{1/2}$; $w = 1/(\sigma(F_o))^2$, $\sigma(F_o) = [\sigma^2(I) + (0.04I)^2]^{1/2}/2F_o$Lp.

Table 4
Fractional atomic coordinates with e.s.d.s in parentheses

Atom	x	y	z
Fe1	0.65204(8)	0.19001(5)	0.74111(5)
Fe2	0.4430(1)	0.07597(5)	0.73715(6)
Fe3	0.50495(9)	0.21200(5)	0.84700(5)
Fe4	0.51092(8)	0.28602(5)	0.72862(5)
P1	0.3314(2)	0.32084(9)	0.72389(9)
P2	−0.0073(2)	0.65553(9)	0.7314(1)
P3	−0.1536(2)	0.77810(9)	0.7884(1)
O11	0.6983(5)	0.1259(4)	0.5765(3)
O12	0.8548(5)	0.3441(3)	0.7749(5)
O13	0.8022(5)	0.1122(3)	0.8231(3)
O21	0.5247(6)	−0.0399(3)	0.8134(4)
O22	0.424(1)	−0.0097(4)	0.5729(4)
O23	0.1716(6)	0.0236(4)	0.7485(4)
O31	0.6078(5)	0.1330(3)	0.9554(3)
O32	0.6229(5)	0.3804(3)	0.9373(3)
O33	0.2605(5)	0.1866(4)	0.9170(3)
O41	0.6634(5)	0.4587(3)	0.7875(3)
O42	0.5380(5)	0.2684(3)	0.5601(3)
N	0.4744(4)	0.1820(3)	0.7360(3)
N1	−0.1177(5)	0.6980(3)	0.7443(3)
C11	0.6804(7)	0.1512(5)	0.6416(4)
C12	0.7704(6)	0.2861(4)	0.7619(5)
C13	0.7417(7)	0.1408(4)	0.7895(4)
C21	0.4932(8)	0.0043(4)	0.7828(5)
C22	0.435(1)	0.0234(5)	0.6380(5)
C23	0.2808(8)	0.0431(4)	0.7460(5)
C31	0.5674(7)	0.1618(4)	0.9108(4)
C32	0.5573(7)	0.3147(4)	0.8984(4)
C33	0.3544(7)	0.1989(4)	0.8875(4)
C41	0.6038(6)	0.3920(4)	0.7650(4)
C42	0.5286(6)	0.2782(3)	0.6283(4)
C111	0.3494(6)	0.4112(3)	0.6818(4)
C112	0.3460(7)	0.3998(4)	0.6005(4)
C113	0.3724(8)	0.4661(4)	0.5648(4)
C114	0.4005(8)	0.5453(4)	0.6119(4)
C115	0.4048(8)	0.5580(4)	0.6922(4)
C116	0.3785(7)	0.4916(4)	0.7274(4)
C121	0.1997(6)	0.2466(4)	0.6592(3)
C122	0.2011(6)	0.1657(4)	0.6308(4)
C123	0.0993(7)	0.1095(4)	0.5829(5)
C124	−0.0030(7)	0.1340(5)	0.5618(5)
C125	−0.0041(7)	0.2152(4)	0.5889(5)
C126	0.0956(6)	0.2708(4)	0.6369(4)
C131	0.2643(6)	0.3451(3)	0.8186(4)
C132	0.3406(6)	0.4032(4)	0.8827(4)
C133	0.2947(7)	0.4192(4)	0.9562(4)
C134	0.1722(7)	0.3758(5)	0.9674(4)
C135	0.0982(7)	0.3190(5)	0.9063(4)
C136	0.1419(6)	0.3034(4)	0.8322(4)
C211	−0.0671(6)	0.5603(3)	0.6572(3)
C212	0.0181(6)	0.5174(4)	0.6227(4)
C213	−0.0329(7)	0.4400(5)	0.5688(4)
C214	−0.1596(7)	0.4092(5)	0.5519(4)
C215	−0.2421(7)	0.4506(4)	0.5841(4)
C216	−0.1960(6)	0.5275(4)	0.6386(4)
C221	0.1271(5)	0.7166(3)	0.6945(3)
C222	0.2089(7)	0.8041(4)	0.6069(4)
C223	0.1075(6)	0.7590(4)	0.6391(4)
C224	0.3299(7)	0.8056(4)	0.6283(4)
C225	0.3512(7)	0.7640(4)	0.6832(4)
C226	0.2507(6)	0.7193(4)	0.7170(4)
C231	0.0455(6)	0.6286(3)	0.8179(3)
C232	0.1094(6)	0.6893(4)	0.8827(4)
C233	0.1448(6)	0.6692(4)	0.9511(4)
C234	0.1172(7)	0.5878(4)	0.9532(4)
C235	0.0552(7)	0.5267(4)	0.8902(4)
C236	0.0164(6)	0.5470(4)	0.8217(4)
C311	−0.0386(6)	0.8460(3)	0.8660(3)
C312	0.0797(6)	0.8878(4)	0.8469(4)
C313	0.1727(7)	0.9336(4)	0.9081(4)
C314	0.1494(7)	0.9371(5)	0.9847(4)
C315	0.0350(7)	0.8960(5)	1.0044(4)
C316	−0.0608(6)	0.8509(4)	0.9447(4)
C321	−0.1835(6)	0.8334(4)	0.7173(3)
C322	−0.1478(7)	0.9185(4)	0.7323(4)
C323	−0.1818(8)	0.9559(5)	0.6741(5)
C324	−0.2499(8)	0.9102(5)	0.6068(5)
C325	−0.2867(8)	0.8261(5)	0.5901(5)
C326	−0.2494(7)	0.7870(4)	0.6466(4)
C331	−0.2978(6)	0.7480(3)	0.8322(3)
C332	−0.3312(6)	0.6743(4)	0.8544(4)
C333	−0.4433(7)	0.6519(4)	0.8918(4)
C334	−0.5187(7)	0.7057(5)	0.9045(4)
C335	−0.4869(7)	0.7771(5)	0.8829(4)
C336	−0.3759(6)	0.8002(4)	0.8466(4)

($\lambda = 0.71073$ Å). The diffracted intensities were corrected for Lorentz polarization and absorption (empirical correction) but not for extinction [22]. Scattering factors for all the atomic species and anomalous dispersions corrections for scattering factors of non-hydrogen atoms were taken from Ref. [23]. The structure was solved by Patterson and Fourier methods and refined by full-matrix least-squares, minimizing the function $\Sigma w(|F_o| - k|F_c|)^2$. An anisotropic thermal parameter was assigned to all the atoms of the anion. The hydrogen atoms were introduced in the structure model at calculated positions (C–H 0.95 Å); no refinement was attempted for these atoms. The final difference Fourier synthesis showed maxima residuals of 0.6 e $Å^{-3}$. The atomic coordinates are listed in Table 4. All the calculations were performed on a HP Vectra 486/33 computer using the Personal SDP Structure Determination Package [24].

Acknowledgement

We acknowledge the MURST (Italy) for financial assistance.

References

[1] P. Zanello, *Coord. Chem. Rev.*, *83* (1988) 199.
[2] P. Zanello, *Coord. Chem. Rev.*, *87* (1988) 1.
[3] P. Zanello, *Struct. Bonding (Berlin)*, *79* (1992) 101.

[4] P. Zanello, in P. Zanello (ed.), *Stereochemistry of Organometallic and Inorganic Compounds*, Vol. 5, Elsevier, Amsterdam, 1994, p. 163.
[5] R. Hourihane, T.R. Spalding, G. Ferguson, T. Deeney and P. Zanello, *J. Chem. Soc., Dalton Trans.*, (1993) 43.
[6] M. Tachikawa, J. Stein, E.L. Mutterties, R.G. Teller, M.A. Beno, E. Gebert and J.M. Williams, *J. Am. Chem. Soc., 102* (1980) 6648.
[7] D.E. Fjare and W.L. Gladfelter, *Inorg. Chem., 20* (1981) 3533.
[8] A. Gourdon and Y. Jeannin, *J. Organomet. Chem., 440* (1992) 353.
[9] D. Astruc, *Angew. Chem., Int. Ed. Engl., 27* (1988) 643.
[10] A.Darchen, C. Mahé and H. Patin, *J. Chem. Soc., Chem. Commun.*, (1982) 243.
[11] H.H. Ohst and J.K. Kochi, *J. Am. Chem. Soc., 108* (1986) 2897.
[12] H.H. Ohst and J.K. Kochi, *Inorg. Chem., 25* (1986) 2066.
[13] G.J. Bezems, P.H. Rieger and S. Visco, *J. Chem. Soc., Chem. Commun.*, (1981) 265.
[14] A.J. Downard, B.H. Robinson and J. Simpson, *Organometallics, 5* (1986) 1140.
[15] M.G. Richmond and J.K. Kochi, *Inorg. Chem., 25* (1986) 656.
[16] J.P. Lozos, B.M. Hoffman and C. G. Franz, *QCPE, 295* (1974) 20.
[17] C.C. Neto, S. Kim, Q. Meng, D.A. Sweigart and Y.K. Chung, *J. Am. Chem. Soc., 115* (1993) 2077.
[18] M.R. Churchill, K.N. Amoh and H.J. Wasserman, *Inorg. Chem., 20* (1981) 1609.
[19] J.D. Atwood, in G.L. Geoffroy (ed.), *Inorganic Chemistry. Inorganic and Organometallic Reaction Mechanisms,* Brooks/Cole, Monterey, CA, 1985, Ch. 4.
[20] C. Bianchini, F. Laschi, D. Masi, F.M. Ottaviani, A. Pastor, M. Peruzzini, P. Zanello and F. Zanobini, *J. Am. Chem. Soc., 115* (1993) 2723.
[21] D.F. Shriver and M.A. Drezdon, *The Manipulation of Air-Sensitive Compounds,* Wiley, New York, 2nd edn., 1986.
[22] A.C. North, D.C. Phillips and F.S. Mathews, *Acta Crystallogr., Sect. A, 24* (1968) 351.
[23] *International Tables for X-Ray Crystallography,* Vol. IV, Kynoch, Birmingham, UK, 1974.
[24] (a) B.A. Frenz, *Comput. Phys., 2* (1988) 42; (b) *Crystallographic Computing 5*, Oxford University Press, Oxford, 1991, Ch. 11, p. 126.